Supporting Information

Unprecedented Lead-Antimony Oxohalide Clusters with the Efficient Capture for UO_2^{2+} Ions

Jia-Hua Luo,[a,b,c] Yu-Wei Ren,[a,b,c] Lu Yang,[b,d] Jing Wang,[b,c,e] Hao-Dan Xiao,[b,c,e] Feng-Hua Xian,[e] Hai-Yan Sun,[b,c,d] Mei-Ling Feng,[b,d,*] Bing Hu,[b,d,*] and Xiao-Ying Huang[b,d]

a. College of Chemistry, Fuzhou University, Fuzhou, Fujian, 350108, China.
b. State Key Laboratory of Structural Chemistry, Fujian Institute of Research on the Structure of Matter, The Chinese Academy of Sciences, Fuzhou, Fujian, 350002, China.
c. Fujian College, University of Chinese Academy of Sciences, Fuzhou, Fujian, 350002, China.
d. University of Chinese Academy of Sciences, Beijing, 100049, China.
e. Fujian Provincial Key Laboratory of Advanced Materials Oriented Chemical Engineering, College of Chemistry and Materials Science, Fujian Normal University, Fuzhou, 350007, China.

1. Experimental Section

Materials

PbI_2 (98%, Adamas Reagent Co., Ltd.), $Sb(CH_3COO)_3$ (99+%, Shanghai Aladdin Biochemical Technology Co., Ltd.), methanol (AR, Sinopharm Chemical Reagent Co., Ltd.), triethanolamine (AR, Sinopharm Chemical Reagent Co., Ltd.), triethylamine (AR, Sinopharm Chemical Reagent Co., Ltd.), $(UO_2)(NO_3)_2·6H_2O$ (99%, Hubei Jusheng Technology Co., Ltd.) and NaOH (AR, General-Reagent). All reagents for synthesis were purchased from commercial sources and used without further purification.

Synthesis

$[(HTEOA)SbOPbI]_4·2H_2O$ (**1**) was prepared as follows: A mixture of $Sb(CH_3COO)_3$ (448.3 mg, 1.5 mmol), PbI_2 (230.5 mg, 0.5 mmol), 5 mL of methanol, 0.2 mL of triethanolamine, and 0.4 mL of triethylamine were added to 20 mL of stainless steel reactor with a Teflon liner in turn, sealed, and heated at 393 K for 3 days and then cooled to room temperature. Many grey prismatic crystals and a moderate amount of yellow solid impurities were obtained. The product was ultrasonically treated and then washed cleaned three times with ethanol and water. Interestingly, when the product was washed with water, it could be observed that the crystals of **1** floated on the water surface, and by rolling using the solid phase and liquid phase pages, the crystals of **1** were enriched on the water surface, and the pure phase of **1** could be collected by repeatedly separating these products. The yield was 24% based on Sb atom. EA: calcd., C: 11.47%, H: 2.25%, N: 2.23%. Found, C: 11.70%, H: 2.28%, N: 2.23%.

$(HTEOA)_3Sb_3OPbI_3·CH_3OH$ (**2**) was prepared using a method analogous to that for the preparation of **1**. The difference arose from the amount of $Sb(CH_3COO)_3$ used, which was adjusted to (149.4 mg, 0.5 mmol), and no triethylamine was added. A medium amount of colourless transparent columnar crystal aggregates and a large amount of yellow solid powder were obtained. The crystals of **2** were then collected by hand-picking under a microscope. The yield was 11% based on Sb atom. EA: calcd., C: 15.82%, H: 3.00%, N: 2.91%. Found, C: 14.91%, H: 2.65%, N: 2.89%. There is a discrepancy in the experimental and calculated EA results for **2**, which might be due to the escape of solvent methanol molecules during actual testing. The calculated EA results after eliminating the influence of methanol are C: 15.15%, H: 2.75%, N: 2.91%.

2. Characterization techniques

Microscopically selected crystals of appropriate size were fixed at the top of glass fiber for single-crystal X-ray diffraction (SCXRD) characterization. SCXRD data of **1** were collected with the graphite-monochromated MoK_α (λ = 0.71073 Å) at 295 K using a Rigaku SuperNova diffractometer. SCXRD data for **2** were collected with a Rigaku XtaLAB-Synergy-R diffractometer with graphite-monochromated MoK_α (λ = 0.71073 Å) at 100 K. The structures were solved by direct methods and refined by full-matrix least-squares on F^2 using the *SHELX*-2019 program package.[1] The empirical formulae were jointly verified by the results of elemental analyses (EA), thermogravimetric analysis (TGA), energy-dispersive spectroscopy (EDS). The crystallographic data of title compounds and refined details are shown in Table S1. Selected bond lengths and angles of compounds are shown in Table S2, S3, and S4. Powder X-ray diffraction (PXRD) patterns were obtained on a Rigaku Miniflex-II diffractometer by using CuK_α radiation (λ = 1.54178 Å) with an angular range of 2θ = 3° - 65° at 30 kV, 15 mA and a step size of 0.27. EA of C, H, and N was performed using a German Elementary Vario

EL III instrument. EDS was obtained by a JEOL JSM-6700F scanning electron microscope. TGA was performed using crystalline samples loaded in Al_2O_3 crucibles with a NETZSCH STA 449F3 unit at a heating rate of 10 $^oC \cdot min^{-1}$ under N_2 atmosphere and in the temperature range of 20 - 800 ^oC. The metal elemental ratios were determined by ICP-Atomic Emission Spectrometry (AES) using an Ultima 2 instrument. Inductively Coupled Plasma-Optical Emission Spectroscopy (ICP-OES) was studied on an ICAP-7400 to measure the metal ions concentrations. The concentrations of uranium were measured by Inductively Coupled Plasma-Mass Spectrometry (ICP-MS) on XSerise II.

3. Uranium adsorption experiments

Due to the different morphology of uranium under different pH conditions, the range of pH in practical applications are different (Fig. S6). In the following adsorption experiments, the pH values of solutions were adjusted in the range from 4.0 to 5.0 to avoid uranium precipitation.

In adsorption isotherm experiments, the polycrystalline powder sample of **1** was added into solutions with different concentrations of UO_2^{2+} (C_0^U = 7.82-895.85 mg/L), respectively. The *V*/*m* values of all samples were 1000 mL/g (*V* = 10 mL, *m* = 10 mg). The adsorption isotherm experiments lasted about 2 hours with continuous stirring at room temperature.

In the kinetic experiments, 50 mg of polycrystalline powder sample of **1** was added to 50 mL (19.92 mg/L) UO_2^{2+} solution (pH = 4.5) under magnetic stirring at room temperature. The mixture was kept under magnetic stirring. The suspensions were sampled at different time intervals at room temperature (0, 1, 2, 5, 10, 15, 20, 30, 60, 100, 120, 300, 600, 660, 1440 minutes for **1**).

In pH-dependent experiments of UO_2^{2+} adsorption, the initial UO_2^{2+} concentration was approximately 5 mg L^{-1}. The pH of various UO_2^{2+} aqueous solutions was adjusted using HNO_3 or NaOH solutions (pH = 2.58-11.57). Adsorption experiments of all samples were performed with *V*/*m* of 1000 mL g^{-1} (*V* = 10 mL, *m* = 10 mg) at room temperature and for 2 h contact time.

In adsorption experiments after irradiation, the pristine powder samples were irradiated by 100 kGy *β*, 200 kGy *β*, 100 kGy *γ*, and 200 kGy *γ* irradiations. A small number of irradiated samples were taken separately and subjected to PXRD to confirm the structural stability. 10 mg of irradiated samples were added to 10 mL of 9.78 mg L^{-1} of UO_2^{2+} aqueous solutions at room temperature and for 2 h contact time.

In competitive ion exchange experiments, solutions with different molar ratios of UO_2^{2+}/M^{n+} (M^{n+} = Na^+, Mg^{2+} and Ca^{2+} ions) and mixed solutions of multiple competing ions were prepared. **1** was added to the as prepared aqueous solutions, respectively. The *V*/*m* ratio is also 1000 mL g^{-1} (*V* = 10 mL, *m* = 10 mg). The mixed solutions were stirred for 2 h at room temperature. In actual water samples, UO_2^{2+} were added to ultrapure water, river water (Wulong River, Fuzhou, Fujian, China), and lake water (Qishan Lake, Fuzhou, Fujian, China).

All above solutions were filtered by the 0.22 μm Millipore filter on the 5 mL syringe and then diluted with 2% HNO_3 to meet the concentration range of the test instrument. The concentrations of UO_2^{2+} were determined by ICP-MS and other ions in aqueous solutions were determined by ICP-OES.

4. Equations

(1) Adsorption isotherm models[2]:

$$q = q_m \frac{bC_e}{1 + bC_e} \qquad (Equation\ S1)$$

$$q_e = K_F C_e^{1/n} \qquad (Equation\ S2)$$

$$q = q_m \frac{(bC_e)^{1/n}}{1 + (bC_e)^{1/n}} \qquad (Equation\ S3)$$

Equations S1, S2, and S3 represent three classical isotherm models, namely the Langmuir (Equation S1), Freundlich (Equation S2), and Langmuir-Freundlich (Equation S3) models. They are used to determine their maximum adsorption capacity (q_m) of **1**. Where q and C_e represent the adsorption amount at time t (min) and the equilibrium ion concentration, respectively; b (L/mg) is Langmuir constant related to the affinity of the ions towards the adsorbents, K_F and n are the Freundlich constant.

(2) Adsorption capacity (q):

$$q = \frac{(C_0 - C_e)V}{m} \qquad (Equation\ S4)$$

Where C_0 and C_e are concentrations of the target ions (mg/L) at the initial state and equilibrium state, respectively. V is the solution volume (mL); m (g) is the mass of **1** used for adsorption.

(3) Removal rate (R):

$$R = \frac{(C_0 - C_e)}{C_0} \times 100\% \qquad (Equation\ S5)$$

Where C_0 and C_e have the same meaning as in Equation S4.

(4) Kinetics models are shown in below[3]:

$$ln\frac{(q_e - q)}{q_e} = -k_1 t \qquad (Equation\ S6)$$

$$\frac{t}{q} = \frac{1}{k_2 q_e^2} + \frac{1}{q_e} t \qquad (Equation\ S7)$$

Equations S6 and S7 represent pseudo-first-order (Equation S6) and the pseudo-second-order (Equation S7) kinetics models. Where q_e (mg/g) and q (mg/g) are the adsorption capacities at equilibrium and time t (min), respectively. Where k_1 and k_2 are pseudo-first-order and the pseudo-second-order rate constant of kinetics models, respectively.

(5) distribution coefficient (K_d):

$$K_d = \frac{V(C_0 - C_e)}{m \quad C_e} \qquad (Equation\ S8)$$

Where C_0 and C_e have the same meaning as in Equation S4; V is the solution volume (mL); m (g) is the mass of **1** used for adsorption.

(6) The separation factor (SF):

$$SF = \frac{K_d^A}{K_d^B} \qquad (Equation\ S9)$$

Where K_d^A (mg L^{-1}) and K_d^B (mg L^{-1}) are the distribution coefficient of A and B ions, respectively.

5. Crystal structures

Table S1. Crystallographic data and refinement details for **1** and **2**.

Compound	1	2
Empirical formula	$C_{24}H_{56}I_4N_4O_{18}Pb_4Sb_4$	$C_{19}H_{43}N_3O_{11}Sb_3I_3Pb$
Formula weight	2512.08	1442.70
Temperature/K	293(2)	100(2)
Crystal system	orthorhombic	orthorhombic
Space group	*Fddd*	$P2_12_12_1$
a/Å	13.5517(17)	12.1178(3)
b/Å	26.077(3)	15.5542(4)
c/Å	31.062(3)	18.9473(5)
α/°	90	90
β/°	90	90
γ/°	90	90
V/Å^3	10977(2)	3571.24(16)
Z	8	4
ρ_{calc}/g cm^{-3}	3.040	2.683
μ/mm^{-1}	16.469	9.589
F (000)	8928.0	2640.0
Crystal size/mm^3	0.18 ×0.18 × 0.13	0.05 × 0.05 × 0.05
Radiation	MoK_α (λ = 0.71073 Å)	MoK_α (λ = 0.71073 Å)
2θ range for data collection/°	5.192 to 48.814	3.99 to 61.578
Index ranges	-15 <= *h* <= 15, -25 <= *k* <= 30, -34 <= *l* <= 36	-15 <= *h* <= 14, -16 <= *k* <= 20, -23 <= *l* <= 22
Reflections collected	13247	22557
Independent reflections	2268 [R_{int} = 0.0715, R_{sigma} = 0.0555]	8403 [R_{int} = 0.0350, R_{sigma} = 0.0425]
Data/restraints/parameters	2268/25/150	8403/5/375
Goodness-of-fit on F^2	1.021	1.045
Final *R* indexes [*I*>=2σ (*I*)]	$^aR_1$ = 0.0431, ^{b}wR_2 = 0.0907	$^aR_1$ = 0.0272, ^{b}wR_2 = 0.0593
Final *R* indexes [all data]	R_1 = 0.0779, wR_2 = 0.1088	R_1 = 0.0314, wR_2 = 0.0608
Largest diff. peak/hole/eÅ^{-3}	1.23/-1.05	1.60/-1.11

CCDC	2513808	2513809

$^{a}R_1 = \sum \| F_o | - | F_c \| / \sum | F_o |$, $^{b}wR_2 = [\sum w(F_o^2 - F_c^2)^2 / \sum w(F_o^2)^2]^{1/2}$.

Table S2. Selected bond distances (Å) for **1** and **2**.

1		**2**	
I(1)-Pb(1)	3.5195(15)	I(1)-Pb(1)	3.1375(6)
I(2)-Pb(1)	3.4992(16)	I(2)-Pb(1)	3.1869(6)
Pb(1)-O(1)#2	2.439(8)	I(3)-Pb(1)	3.1048(6)
Pb(1)-O(1)	2.374(9)	Pb(1)-O(4)	2.672(6)
Pb(1)-O(1)#3	2.368(9)	Pb(1)-O(7)	2.583(6)
Pb(1)-O(2)	2.726(10)	Pb(1)-O(10)	2.615(5)
Pb(1)-O(3)#3	2.751(10)	Sb(1)-O(1)	2.081(6)
Sb(1)-O(1)	2.008(8)	Sb(1)-O(2)	2.035(5)
Sb(1)-O(2)	1.999(11)	Sb(1)-O(3)	3.004(6)
Sb(1)-O(3)	1.988(11)	Sb(1)-O(4)	2.000(6)
Sb(1)-N(1)	2.578(13)	Sb(1)-N(1)	2.486(7)
		Sb(2)-O(1)	2.100(5)
		Sb(2)-O(5)	2.018(6)
		Sb(2)-O(6)	2.937(7)
		Sb(2)-O(7)	1.987(6)
		Sb(2)-N(2)	2.435(6)
		Sb(3)-O(1)	2.110(5)
		Sb(3)-O(8)	2.010(6)
		Sb(3)-O(9)	3.013(6)
		Sb(3)-O(10)	1.996(5)
		Sb(3)-N(3)	2.431(7)

Symmetry codes: #2 3/4-*x*, +*y*, 3/4-*z*; #3 3/4-*x*, 3/4-*y*, +*z*; #4 1/4-*x*, 5/4-*y*, +*z*.

Table S3. Selected bond angles (Å) for **1** and **2**.

1			
I(2)-Pb(1)-I(1)	121.958(16)	O(1)-Pb(1)-O(3)#3	106.6(3)
O(1)#3-Pb(1)-I(1)	138.4(2)	O(1)#3-Pb(1)-O(3)#3	62.4(3)
O(1)-Pb(1)-I(1)	73.7(2)	O(2)-Pb(1)-I(1)	75.1(2)
O(1)#2-Pb(1)-I(1)	73.1(2)	O(2)-Pb(1)-I(2)	151.8(2)
O(1)-Pb(1)-I(2)	139.8(2)	O(2)-Pb(1)-O(3)#3	80.2(3)
O(1)#3-Pb(1)-I(2)	75.5(2)	O(3)#3-Pb(1)-I(1)	152.0(2)
O(1)#2-Pb(1)-I(2)	74.7(2)	O(3)#3-Pb(1)-I(2)	76.6(2)
O(1)-Pb(1)-O(1)#2	76.1(3)	O(1)-Sb(1)-N(1)	144.7(4)
O(1)#3-Pb(1)-O(1)	77.0(3)	O(2)-Sb(1)-O(1)	83.8(4)
O(1)#3-Pb(1)-O(2)	107.5(3)	O(2)-Sb(1)-N(1)	73.6(5)
O(1)-Pb(1)-O(2)	62.9(3)	O(3)-Sb(1)-O(1)	83.9(4)
O(1)#2-Pb(1)-O(2)	133.5(3)	O(3)-Sb(1)-O(2)	97.2(5)
O(1)#2-Pb(1)-O(3)#3	134.8(3)	O(3)-Sb(1)-N(1)	72.8(4)

Symmetry codes: #2 3/4-*x*, +*y*, 3/4-*z*; #3 3/4-*x*, 3/4-*y*, +*z*.

2			
I(1)-Pb(1)-I(2)	102.594(17)	O(4)-Sb(1)-N(1)	74.4(2)
I(3)-Pb(1)-I(1)	92.208(17)	N(1)-Sb(1)-O(3)	63.6(2)
I(3)-Pb(1)-I(2)	92.628(17)	O(1)-Sb(2)-O(6)	142.83(19)
O(4)-Pb(1)-I(1)	166.70(13)	O(1)-Sb(2)-N(2)	144.4(2)
O(4)-Pb(1)-I(2)	90.14(13)	O(5)-Sb(2)-O(1)	76.9(2)
O(4)-Pb(1)-I(3)	91.02(12)	O(5)-Sb(2)-O(6)	139.6(2)
O(7)-Pb(1)-I(1)	83.48(13)	O(5)-Sb(2)-N(2)	76.3(2)
O(7)-Pb(1)-I(2)	171.38(12)	O(7)-Sb(2)-O(1)	84.6(2)
O(7)-Pb(1)-I(3)	93.26(11)	O(7)-Sb(2)-O(5)	97.2(2)
O(7)-Pb(1)-O(4)	83.46(18)	O(7)-Sb(2)-O(6)	83.8(2)
O(7)-Pb(1)-O(10)	87.16(16)	O(7)-Sb(2)-N(2)	76.0(2)
O(10)-Pb(1)-I(1)	90.74(13)	N(2)-Sb(2)-O(6)	64.7(2)
O(10)-Pb(1)-I(2)	86.64(12)	O(1)-Sb(3)-O(9)	143.8(2)
O(10)-Pb(1)-I(3)	177.05(13)	O(1)-Sb(3)-N(3)	145.7(2)
O(10)-Pb(1)-O(4)	86.12(17)	O(8)-Sb(3)-O(1)	77.3(2)
O(1)-Sb(1)-O(3)	145.63(19)	O(8)-Sb(3)-O(9)	138.4(2)
O(1)-Sb(1)-N(1)	145.4(2)	O(8)-Sb(3)-N(3)	77.0(2)
O(2)-Sb(1)-O(1)	79.0(2)	O(10)-Sb(3)-O(1)	85.0(2)
O(2)-Sb(1)-O(3)	135.4(2)	O(10)-Sb(3)-O(8)	96.8(2)
O(2)-Sb(1)-N(1)	76.2(2)	O(10)-Sb(3)-O(9)	84.9(2)
O(4)-Sb(1)-O(1)	85.7(2)	O(10)-Sb(3)-N(3)	75.9(2)
O(4)-Sb(1)-O(2)	98.2(2)	N(3)-Sb(3)-O(9)	63.1(2)
O(4)-Sb(1)-O(3)	89.3(2)		

Table S4. Hydrogen bonds for **2**.

D-H···A	d(D-H) (Å)	d(H···A) (Å)	d(D···A) (Å)	<(DHA) (°)
O(3)-H(3)···I(2)#1	0.824(14)	2.81(5)	3.595(6)	159(11)
O(6)-H(6)···O(2)#2	0.822(14)	1.99(4)	2.784(8)	162(11)
O(9)-H(9)···O(11)	0.818(14)	2.08(8)	2.750(10)	139(11)
C(2)-H(2B)···I(3)#3	0.99	3.25	3.960(9)	130.4
C(3)-H(3A)···I(1)#4	0.99	3.26	4.213(9)	162.3
C(6)-H(6A)···O(3)	0.99	2.60	3.273(12)	125.7

D-H···A	d(D-H) (Å)	d(H···A) (Å)	d(D···A) (Å)	<(DHA) (°)
C(8)-H(8B)···I(2)#1	0.99	3.13	4.083(9)	160.9
C(9)-H(9A)···I(1)#5	0.99	3.29	4.129(9)	143.2
C(9)-H(9B)···I(3)#6	0.99	3.17	4.132(9)	163.2
C(10)-H(10A)···O(9)#2	0.99	2.50	3.483(11)	169.3
C(11)-H(11B)···I(1)#5	0.99	2.99	3.850(8)	145.7
C(12)-H(12A)···O(6)	0.99	2.40	3.088(11)	125.7
C(12)-H(12B)···I(1)	0.99	3.12	3.747(8)	122.2
C(13)-H(13A)···O(5)#2	0.99	2.52	3.317(11)	137.3
C(13)-H(13B)···I(3)#7	0.99	3.16	4.083(8)	155.5
C(14)-H(14A)···I(1)	0.99	3.24	4.226(8)	177.5
C(15)-H(15B)···I(2)#8	0.99	3.07	3.928(9)	146.1
C(16)-H(16B)···I(1)#7	0.99	3.23	3.868(9)	124.1
C(17)-H(17A)···I(1)	0.99	3.21	4.043(8)	143.4
C(18)-H(18A)···O(9)	0.99	2.44	3.136(10)	126.9
C(18)-H(18B)···I(2)	0.99	3.28	3.971(9)	128.8
C(19)-H(19B)···I(1)#8	0.98	3.30	4.105(11)	140.3

Symmetry codes: #1 -*x*, 1/2+*y*, 1/2-*z*; #2 1/2+*x*, 3/2-*y*, -*z*; #3 -*x*, -1/2+*y*, 1/2-*z*; #4 -1+*x*, +*y*, +*z*; #5 1-*x*, 1/2+*y*, 1/2-*z*; #6 1/2-*x*, 2-*y*, -1/2+*z*; #7 1-*x*, -1/2+*y*, 1/2-*z*; #8 1/2-*x*, 1-*y*, -1/2+*z*.

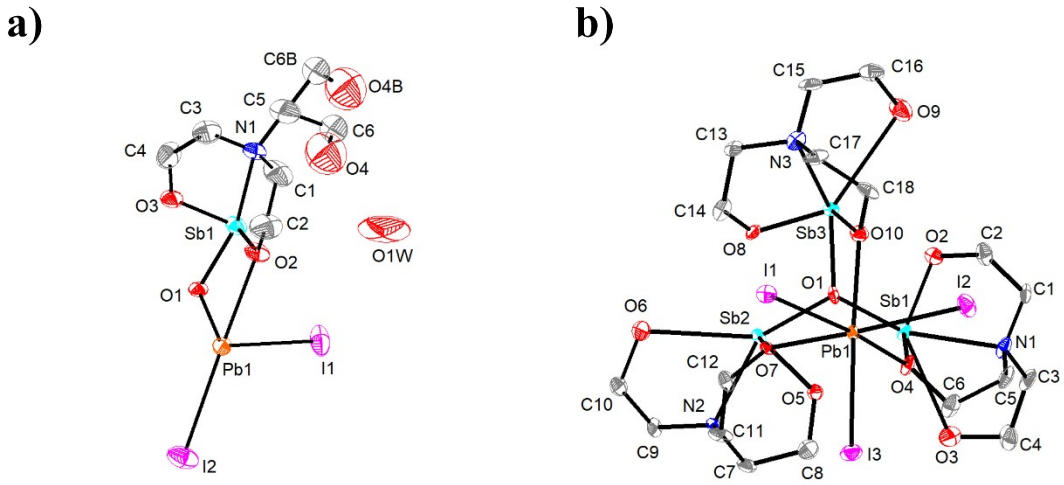

Fig. S1 *ORTEP* plots showing the crystallographically asymmetric units of **1** (a) and **2** (b). Thermal ellipsoids are set at 50% probability level. Hydrogen atoms are omitted for clarity.

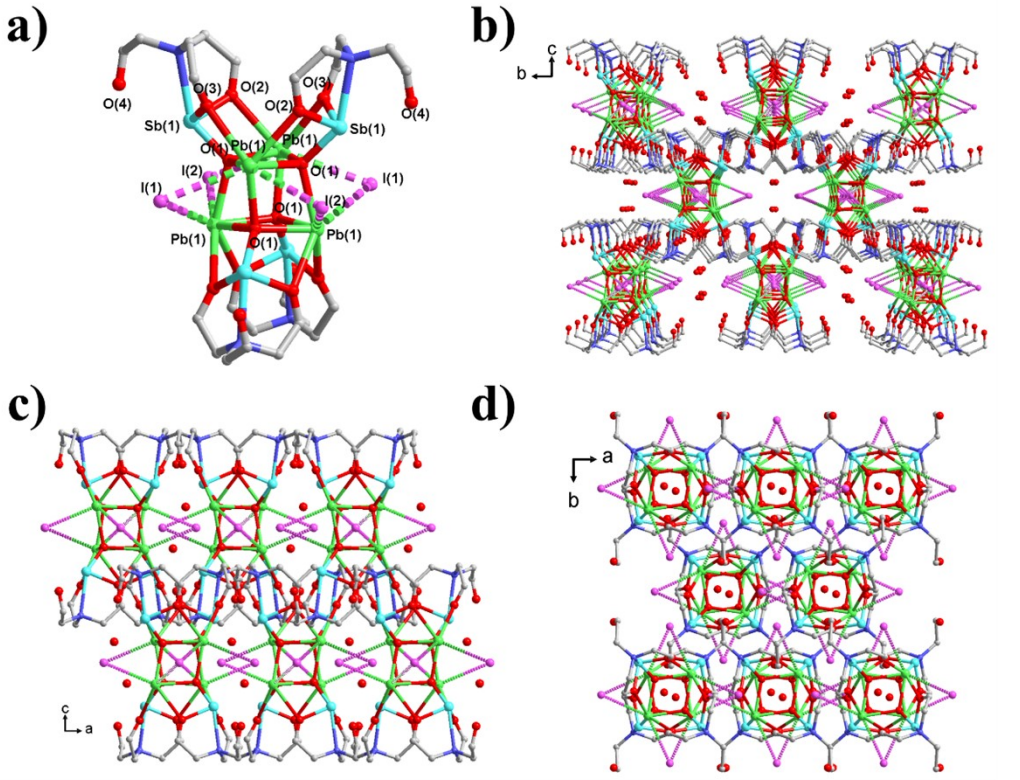

Fig. S2 The structure of the cluster in compound **1** (a) and packing diagrams of **1** viewed along the crystallographic *a* (b), *b* (c), and *c* (d) axes, respectively. Hydrogen atoms are omitted for clarity.

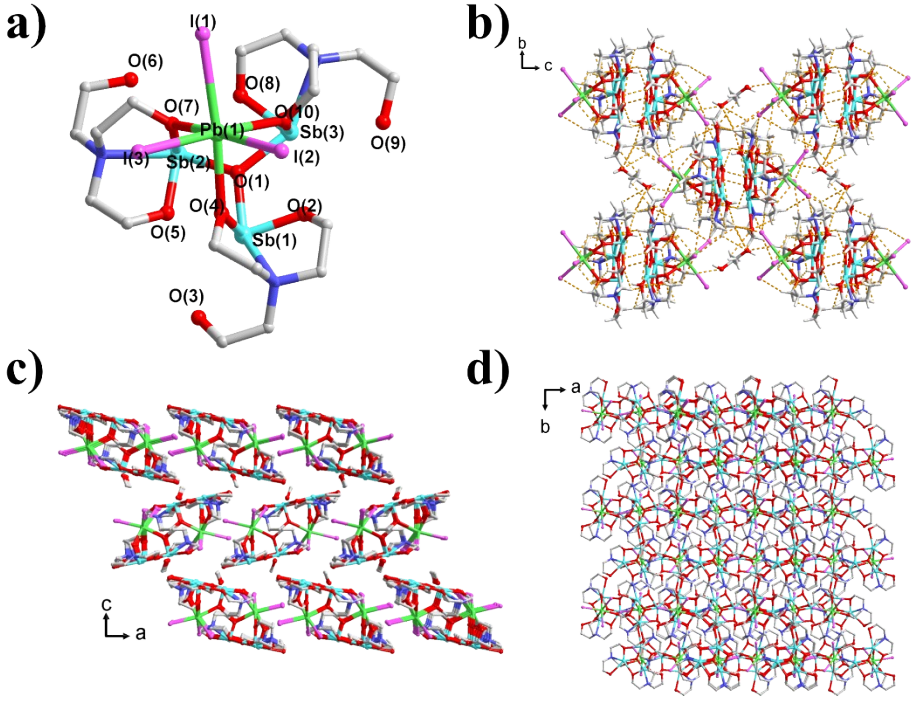

Fig. S3 The structure of the cluster in compound **2** (a) and packing diagrams of **2** viewed along the crystallographic *a* (b), *b* (c), and *c* (d) axes, respectively. Hydrogen bonds are indicated by yellow dashed lines.

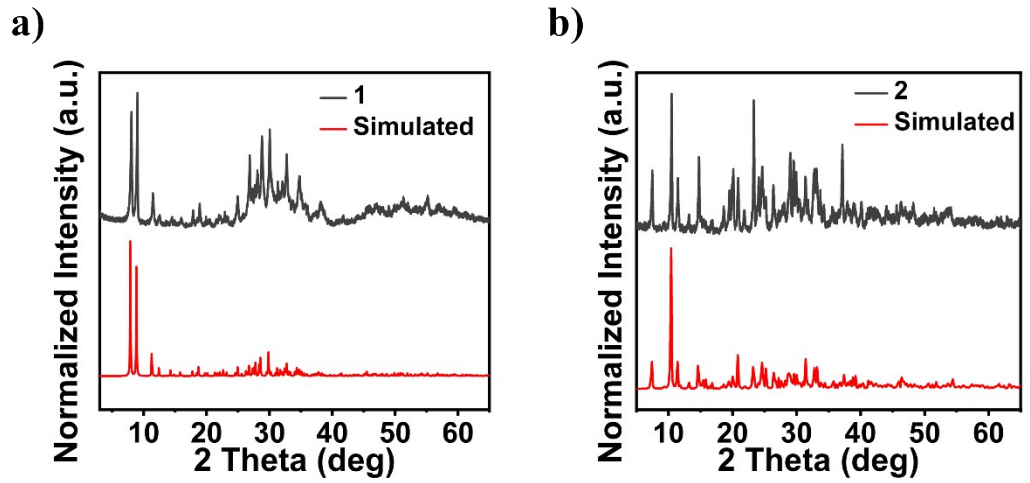

Fig. S4 Simulated and experimental PXRD patterns for **1** (a) and **2** (b).

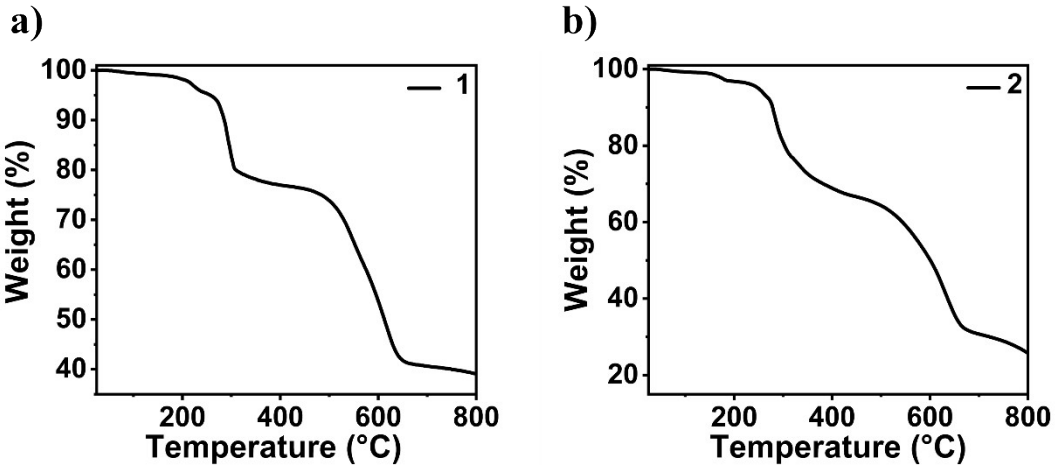

Fig. S5 TG curves for **1** (a) and **2** (b).

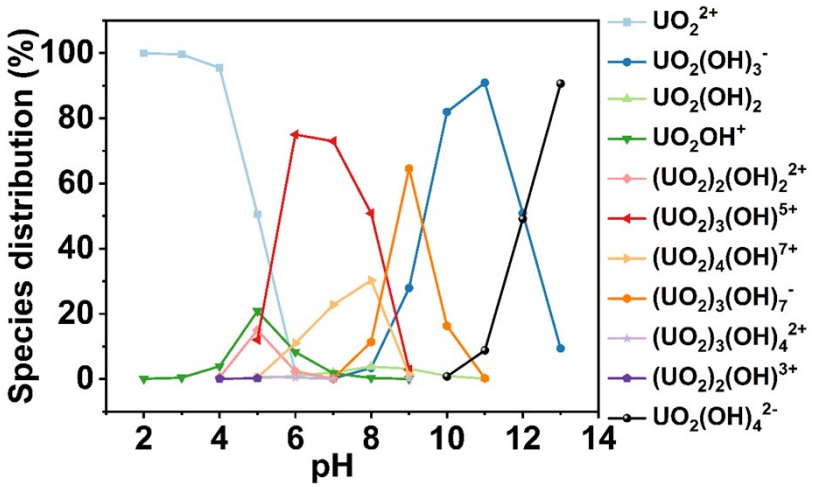

Fig. S6 Distribution of uranium species in aqueous solution at different pH calculated by Visual MINEQL, NIST database (initial uranium concentration of UO_2^{2+} = 5.0 mg/L, at 25 °C).

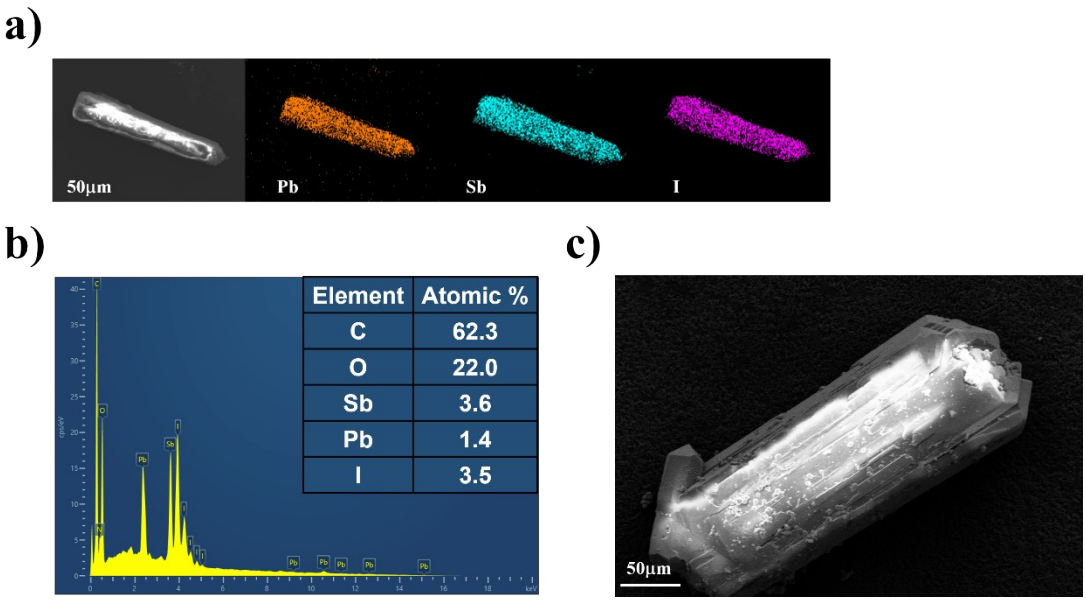

Fig. S7 (a) Elemental distributions mapping, (b) EDS analysis results, and (c) the SEM image of compound **2**.

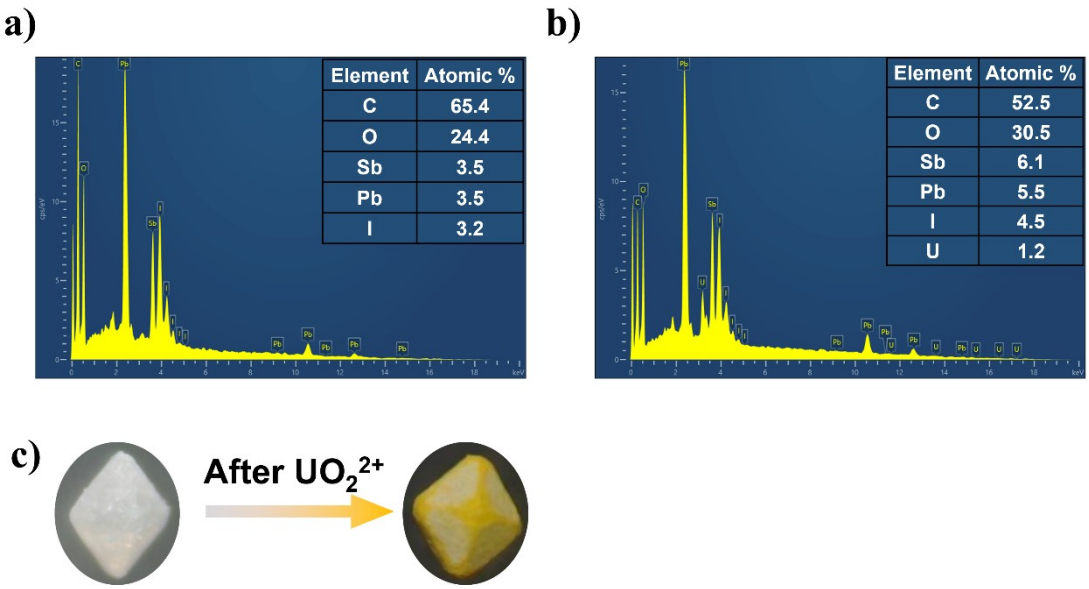

Fig. S8 EDS analysis results of **1** before (a) and after (b) UO_2^{2+} adsorption, and macroscopic crystal changes before and after adsorption (c).

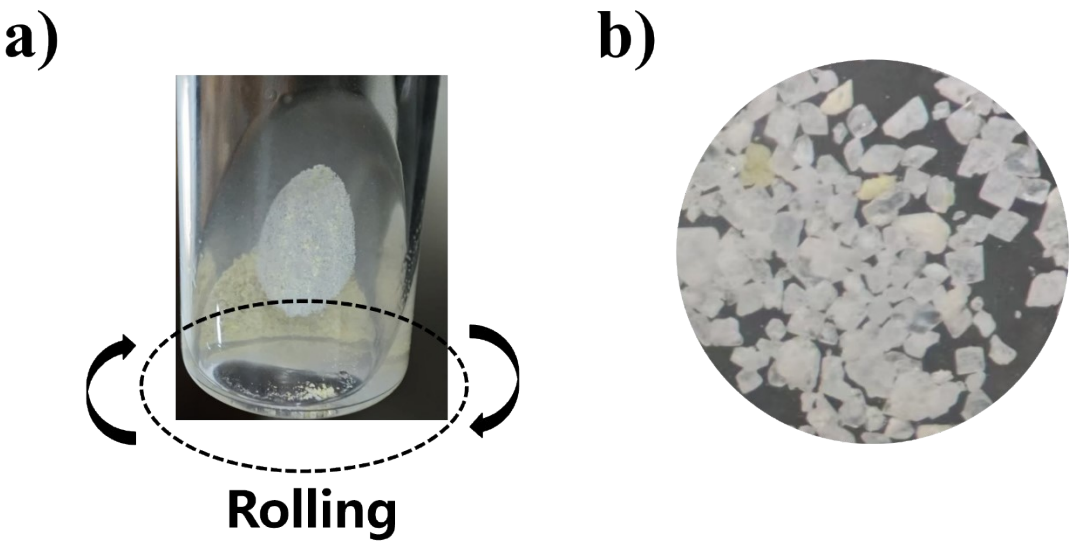

Fig. S9 a) Schematic diagram of rolling collection of crystals **1** using the flotation method. b) Crystals **1** suspended in the upper layer of the liquid.

6. Adsorption isotherm

Table S5. Experimental results of the adsorption capacity study of **1** for UO_2^{2+} (V/m = 1000 mL g^{-1}, at room temperature, and for 2 h contact time).

C_0^U (mg L^{-1})	C_e^U (mg L^{-1})	q^U (mg g^{-1})
7.815	0.0115	7.8035
19.92	0.011	19.909
34.75	0.0115	34.7385
110.2	0.25	109.95
163.95	0.35	163.6
222.35	9.35	213
325.2	79.45	245.75
440.6	167.05	273.55
683.6	418.25	265.35
895.85	607.65	288.2

Table S6. Isotherm fitting parameters of **1** for UO_2^{2+} adsorption (V/m = 1000 mL g^{-1}, at room temperature, and for 2 h contact time).

Adsorption isotherm model	Langmuir model	Langmuir-Freundlich model	Freundlich model
R^2	0.9644	0.9739	0.8823
q_m^U (mg g^{-1})	259.617±10.166	270.125±12.691	-
b (L mg^{-1})	3.775±0.971	2.773±1.128	-
n	-	1.626±0.355	6.993±1.278
k	-	-	123.157±16.947

7. Kinetics

Table S7. The UO_2^{2+} adsorption kinetics results of **1** (V/m = 1000 mL g^{-1}, at room temperature).

Time （minutes）	C_t^U (mg L^{-1})	R^U (%)
0	19.92	0
1	6.14	69.17
2	2.13	89.31
5	0.02	99.89
10	0.01	99.94
15	0.01	99.94
20	0.01	99.94
30	0.01	99.94
60	0.01	99.94
100	0.01	99.94
120	0.01	99.94

	600	0.01	99.94
Time	（minutes）	C_t^U (mg L^{-1})	R^U (%)
	660	0.01	99.94
	1440	0.01	99.94

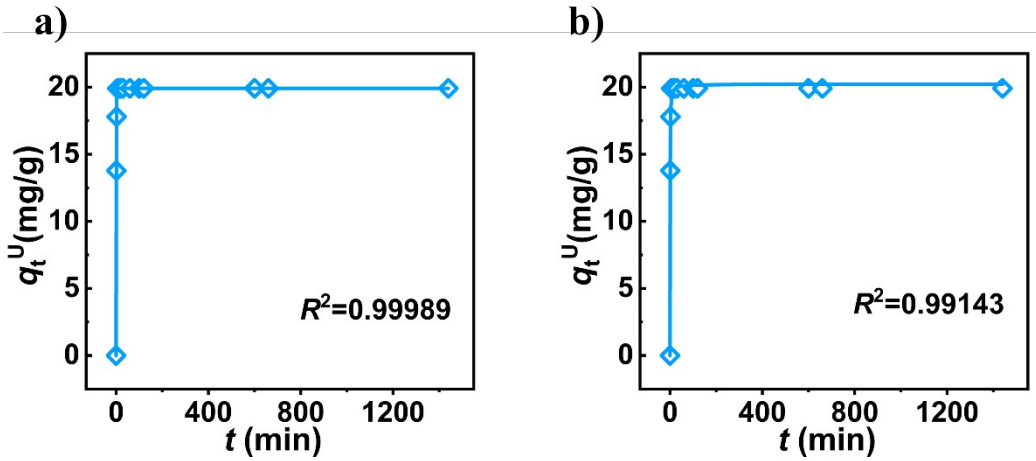

Fig. S10 Pseudo-first-order model kinetics model (a) and pseudo-second-order model (using nonlinear equations) (b) fitted curves for the kinetic data of **1** on UO_2^{2+}.

Table S8. Kinetic fitting parameters of **1** for UO_2^{2+} removal (V/m = 1000 mL g^{-1}, at room temperature).

	k_1 (min^{-1})	k_2 ($g \cdot mg^{-1} \cdot min^{-1}$)	q_e^{Cs} ($mg \cdot L^{-1}$)	R^2
Pseudo-first-order model	1.16183		19.9063	0.99989
Pseudo-second-order model	-	0.13248	20.2166	0.99143

8. pH effect

Table S9. The pH effect adsorption results of **1** for UO_2^{2+} adsorption (V/m = 1000 mL g^{-1}, at room temperature and for 2 h contact time).

pH	C_0^U (mg L^{-1})	$\pm C_0^U$ (mg L^{-1})	C_e^U (mg L^{-1})	$\pm C_e^U$ (mg L^{-1})	K_d^U (mL g^{-1})	$\pm K_d^U$ (mL g^{-1})	R^U (%)	$\pm R$ (%)
2.58	4.777	0.0170	4.211	0.0127	134.410	7.46	11.85	0.5796
4.26	4.814	0.0155	0.014	0.0014	342857.1	33796.08	99.71	0.0284
5.25	4.505	0.0057	0.012	0.0014	374416.7	44077.97	99.73	0.0310
8.06	4.582	0.0134	0.023	0	198195.7	584.13	99.50	0.0015
10.00	4.590	0.0141	0.012	0.0007	398130.4	23355.95	99.75	0.0146
11.57	4.669	0.0021	0.189	0.0007	23766.58	81.65	95.96	0.0133

9. Irradiation effect

Table S10. The results of UO_2^{2+} adsorption for **1** after irradiation (V/m = 1000 mL g^{-1}; at room temperature and for 2 h contact time).

	C_0^U (mg L^{-1})	$\pm C_0$ (mg L^{-1})	C_e^U (mg L^{-1})	$\pm C_e$ (mg L^{-1})	K_d^U (mL g^{-1})	$\pm K_d$ (mL g^{-1})	R^U (%)	$\pm R$ (%)
100kGyβ irradiation	9.78	0.0499	0.0439	0.0002	2216771.4	114372.21	99.9549	0.0023
200 kGy β irradiation	9.78	0.0499	0.0415	0.0002	2347145.5	92893.01	99.9574	0.0017
100 kGy γ irradiation	9.78	0.0499	0.0448	0.0001	2174889.4	63576.81	98.9540	0.0013
200 kGy γ irradiation	9.78	0.0499	0.0432	0.0002	2256311.1	98897.40	98.9557	0.0019

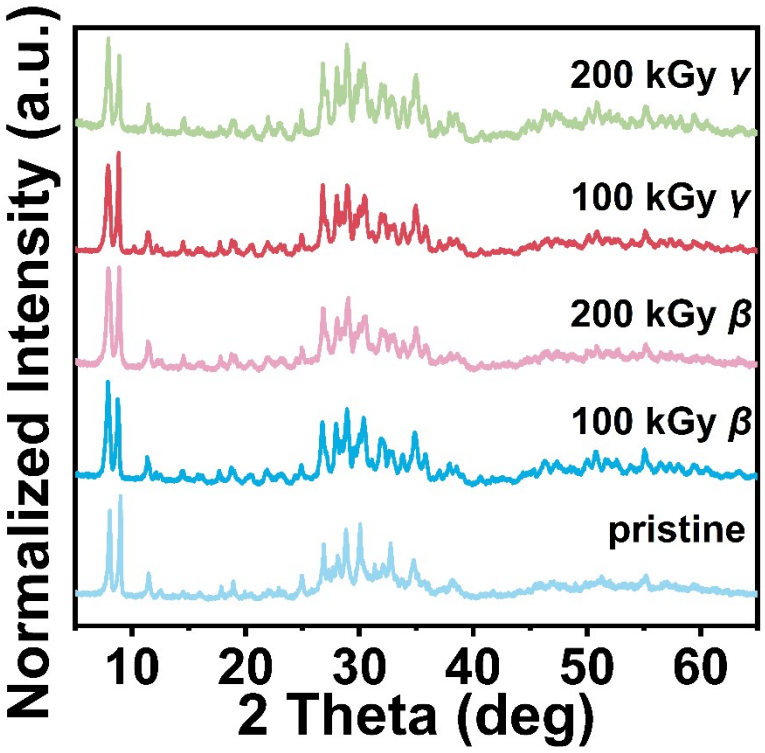

Fig. S11 PXRD patterns of compound **1** before and after irradiation with 100 kGy β and γ radiations and 200 kGy β and γ radiations, respectively.

10. Competitive adsorption

Table S11. The UO_2^{2+} and Na^+ adsorption results of **1** under different Na/U molar ratios (V/m = 1000 mL g^{-1}, at room temperature and for 2 h contact time).

Molar Ratios (Na/U)	UO_2^{2+}	C_0 (mg L^{-1})	$\pm C_0$ (mg L^{-1})	C_e (mg L^{-1})	$\pm C_e$ (mg L^{-1})	K_d (mL g^{-1})	$\pm K_d$ (mL g^{-1})	R (%)	$\pm R$ (%)	
129.30		6.92	0.0182	0.02	0.0006	332520.41	9328.93	99.70	0.0084	
572.18		5.00	0.0106	0.04	0.0007	132373.33	2232.47	99.25	0.1255	
11588.90		4.59	0.0106	0.06	0	74204.92	173.88	98.67	0.0031	
	Na^+	C_0 (mg L^{-1})	$\pm C_0$ (mg L^{-1})	C_e (mg L^{-1})	$\pm C_e$ (mg L^{-1})	K_d (mL g^{-1})	$\pm K_d$ (mL g^{-1})	R (%)	$\pm R$ (%)	$SF_{U/Na}$
		86.36	0.7267	86.32	0.0450	0.56	7.90	0.06	0.7889	591900.71
		276.40	0.0359	271.42	3.0172	18.35	11.19	1.80	1.0788	7213.01
		5134.82	38.4242	5100.58	36.8374	6.71	0.26	0.67	0.0259	11051.50

Table S12. The UO_2^{2+} and Ca^{2+} adsorption results of **1** under different Ca/U molar ratios (V/m = 1000 mL g^{-1}, at room temperature and for 2 h contact time).

Molar Ratios (Ca/U)	UO_2^{2+}	C_0 (mg L^{-1})	$\pm C_0$ (mg L^{-1})	C_e (mg L^{-1})	$\pm C_e$ (mg L^{-1})	K_d (mL g^{-1})	$\pm K_d$ (mL g^{-1})	R (%)	$\pm R$ (%)	
1.05		6.89	0.0145	0.02	0.0008	340418.19	2015.15	99.71	0.0017	
53.92		6.85	0.0727	0.03	0.0003	247769.80	390.13	99.60	0.0006	
482.30		5.16	0.0014	0.02	0.0021	277702.70	32092.25	99.64	0.0410	
	Ca^{2+}	C_0 (mg L^{-1})	$\pm C_0$ (mg L^{-1})	C_e (mg L^{-1})	$\pm C_e$ (mg L^{-1})	K_d (mL g^{-1})	$\pm K_d$ (mL g^{-1})	R (%)	$\pm R$ (%)	$SF_{U/Ca}$
		1.22	0.0124	1.18	0.0002	3.15	1.07	3.15	0.1001	10468.67
		62.21	0.3719	59.85	0.1928	3.79	2.87	3.79	0.2652	6283.64
		418.70	0.1406	415.99	0.7410	0.65	1.45	0.64	0.1436	42600.84

Table S13. The UO_2^{2+} and Mg^{2+} adsorption results of **1** under different Mg/U molar ratios (V/m = 1000 mL g^{-1}, at room temperature and for 2 h contact time).

Molar Ratios (Mg/U)	UO_2^{2+}	C_0 (mg L^{-1})	$\pm C_0$ (mg L^{-1})	C_e (mg L^{-1})	$\pm C_e$ (mg L^{-1})	K_d (mL g^{-1})	$\pm K_d$ (mL g^{-1})	R (%)	$\pm R$ (%)	
1.16		5.14	0.0368	0.010	0.0007	539526.32	36463.14	99.81	0.0124	
43.11		6.88	0.0496	0.023	0.0005	301098.83	8792.93	99.67	0.0096	
285.91		10.15	0.1442	0.002	0.0007	698963.28	24215.01	99.86	0.0049	
	Mg^{2+}	C_0 (mg L^{-1})	$\pm C_0$ (mg L^{-1})	C_e (mg L^{-1})	$\pm C_e$ (mg L^{-1})	K_d (mL g^{-1})	$\pm K_d$ (mL g^{-1})	R (%)	$\pm R$ (%)	$SF_{U/Mg}$
		0.62	0.0209	0.62	0.00005	10.94	3.3726	1.08	0.3300	49326.24
		30.28	0.0281	30.17	0.09998	3.74	2.3940	0.37	0.2376	80597.24
		296.30	2.4531	296.09	0.04259	0.70	8.4288	0.07	0.8417	1001213.40

Table S14. The results on UO_2^{2+} removal by **1** in actual water samples contaminated with UO_2^{2+} (V/m = 1000 mL g^{-1}, at room temperature and for 2 h contact time).

Water	C_0 (mg L^{-1})	$\pm C_0$ (mg L^{-1})	C_e (mg L^{-1})	$\pm C_e$ (mg L^{-1})	K_d (mL g^{-1})	$\pm K_d$ (mL g^{-1})	R (%)	$\pm R$ (%)
Tap water	4.56	0.0134	0.02	0.0035	259714.29	52985.87	99.62	0.0764
Wulong River	4.52	0.0021	0.02	0	300233.33	141.42	99.66	0.0001
Qishan Lake	5.05	0.0120	0.01	0.0007	403200.00	23864.85	99.75	0.1458

Table S15. The comparison of adsorption equilibrium time and removal rates of **1** and various cluster-based materials.

Materials	q_{max} (mg g^{-1})	Equilibrium time (min)	Removal rate (%)	Reference
This Work	282.82	5	99.94	-
SCU-19	587.15	750	91	4
FJSM-CA	121.91	20	57.60	5
FZU-1	57.59	1440	98.5	6
Co-POM	232.04	180	unmentioned	7

References

1 G. M. Sheldrick, Crystal Structure Refinement with SHELXL *Acta Crystallogr. C.*, 2015, **71**, 3-8.

2 K. Sakadevan and H. J. Bavor, Phosphate Adsorption Characteristics of Soils, Slags and Zeolite to be Used as Substrates in Constructed Wetland Systems, *Water Res.*, 1998, **32**, 393-399.

3 Y. S. Ho, D. A. J. Wase and C. F. Forster, Kinetic Studies of Competitive Heavy Metal Adsorption by Sphagnum Moss Peat, *Environ. Technol.*, 1996, **17**, 71-77.

4 H. L. Zhang, W. Liu, A. Li, D. Zhang, X. Y. Li, F. W. Zhai, L. H. Chen, L. Chen, Y. L. Wang and S. A. Wang, Three Mechanisms in One Material: Uranium Capture by a Polyoxometalate-Organic Framework through Combined Complexation, Chemical Reduction, and Photocatalytic Reduction, *Angew. Chem. Int. Ed.*, 2019, **58**, 16110-16114.

5 W. Ma, B. Hu, J. L. Li, Z. Z. Zhang, X. Zeng, J. C. Jin, Z. Li, S. T. Zheng, M. L. Feng and X. Y. Huang, The Uptake of Hazardous Metal Ions into a High-Nuclearity Cluster-Based Compound with Structural Transformation and Proton Conduction, *ACS Appl. Mater. Interfaces*, 2020, **12**, 26222-26231.

6 Y. X. Liu, L. Jia, Y. R. Li, P. W. Cai, M. R. Ou, C. Sun and S. T. Zheng, Bridging Uranium Uptake and PET Plastics Degradation Within an All-Inorganic Polyoxoniobate Framework, *Adv. Funct. Mater.*, 2025, e16939.

7 X. W. Han, Y. Q. Wang, X. H. Cao, Y. Dai, Y. H. Liu, Z. M. Dong, Z. B. Zhang and Y. H. Liu, Adsorptive Performance of Ship-Type Nano-Cage Polyoxometalates for U(VI) in Aqueous Solution, *Appl. Surf. Sci.*, 2019, **484**, 1035-1040.